Nanoscale Advances

ROYAL SOCIETY OF CHEMISTRY

MINIREVIEW

View Article Online
View Journal | View Issue

Cite this: *Nanoscale Adv.*, 2020, **2**, 3069

Multinary copper-based chalcogenide nanocrystal systems from the perspective of device applications

Soubantika Palchoudhury, *[a] Karthik Ramasamy [b] and Arunava Gupta *[c]

Multinary chalcogenide semiconductor nanocrystals are a unique class of materials as they offer flexibility in composition, structure, and morphology for controlled band gap and optical properties. They offer a vast selection of materials for energy conversion, storage, and harvesting applications. Among the multinary chalcogenides, Cu-based compounds are the most attractive in terms of sustainability as many of them consist of earth-abundant elements. There has been immense progress in the field of Cu-based chalcogenides for device applications in the recent years. This paper reviews the state of the art synthetic strategies and application of multinary Cu-chalcogenide nanocrystals in photovoltaics, photocatalysis, light emitting diodes, supercapacitors, and luminescent solar concentrators. This includes the synthesis of ternary, quaternary, and quinary Cu-chalcogenide nanocrystals. The review also highlights some emerging experimental and computational characterization approaches for multinary Cu-chalcogenide semiconductor nanocrystals. It discusses the use of different multinary Cu-chalcogenide compounds, achievements in device performance, and the recent progress made with multinary Cu-chalcogenide nanocrystals in various energy conversion and energy storage devices. The review concludes with an outlook on some emerging and future device applications for multinary Cu-chalcogenides, such as scalable luminescent solar concentrators and wearable biomedical electronics.

Received 18th May 2020
Accepted 18th June 2020

DOI: 10.1039/d0na00399a

rsc.li/nanoscale-advances

Introduction

Multinary semiconductors offer the unique possibility of composition-controlled optoelectronic properties that are widely beneficial for modern electronics, energy storage, and biomedical devices.[1–3] For example, accurate band alignment in

[a]*Civil and Chemical Engineering Department, University of Tennessee at Chattanooga, TN, USA. E-mail: soubantika-palchoudhury@utc.edu*
[b]*UbiQD Inc, Los Alamos, NM, USA*
[c]*Department of Chemistry and Biochemistry, The University of Alabama, AL, USA. E-mail: agupta@ua.edu*

Soubantika Palchoudhury received her B.Tech in Chemical Engineering from the National Institute of Technology, Durgapur, India. She continued her graduate studies in chemical engineering and Inorganic Nanochemistry at The University of Alabama (UA), where she earned her M.S. and Ph.D. in 2012. She received postdoctoral trainings at Yale, the University of South Carolina, and UA. She joined the University of Tennessee in Chattanooga in 2015, where she is now an Assistant Professor in Chemical Engineering. Her group focuses on developing new materials for photonic devices, drug delivery, and environmental applications using methods at the interface of nanochemistry, biomimetics, and material characterization.

Karthik Ramasamy received his PhD from the University of Manchester, UK and did postdoc positions at the University of Alabama and at the Los Alamos National Laboratory. He is currently a Senior Director of Chemistry at UbiQD, Inc, where he leads research and development and manufacturing of quantum dots. His research interests are quantum dots, metal chalcogenide nanocrystals and thin films for energy generation and storage applications.

$CuIn_{1-x}Ga_xSe_{1-y}S_y$ thin film photovoltaics is achievable through variation of the In(Ga) and Se(S) contents.[4] Cu_2ZnSnS_4 nanocrystals have revolutionized solar light harvesting devices over the past decade in terms of sustainability as they comprise earth-abundant elements.[5] Cu-doped luminescent semiconductors have played a key role in modern solid-state lighting and display.[6] In fact, multicomponent Cu-chalcogenides are the most promising class of emerging semiconductor materials for devices in terms of achieving the desired optoelectronic properties using non-toxic and earth-abundant elements.[7] Stroyuk *et al.* summarized some of the multinary Cu-chalcogenide semiconductors, specifically for solar light harvesting applications.[3] Chen *et al.* showed the use of ternary Cu-chalcogenides for water splitting reactions for hydrogen generation.[8] Chang *et al.* highlighted size, shape, and phase-controlled synthesis strategies for semiconductor Cu-chalcogenides in different organic solvents.[9] Coughlan *et al.* provided a detailed overview of the synthesis, assembly, and applications of binary, ternary, and the Cu-III–VI and Cu-II–IV–VI quaternary systems of Cu-chalcogenides.[2] Nevertheless, there have been key advances in quaternary and quinary Cu-based semiconductor nanocrystals as well as their applications in supercapacitor and luminescent solar concentrators in recent years, which are highlighted in this review. This review highlights the scope of multinary Cu-chalcogenide nanocrystals for sustainable energy applications. It summarizes the recent advancements in synthetic approaches to realize ternary, quaternary, and quinary Cu-chalcogenide semiconductor compositions at the nano scale and their application in devices. We have focused on compounds containing S and Se as the chalcogen anions in this review. The review will also introduce some emerging characterization methods to probe the properties of multinary chalcogenide nanocrystals. Finally, special focus will be laid on the various established and new application areas for multicomponent Cu-chalcogenides in the fields of energy harvesting, energy conversion, sustainability, and biomedical electronics.

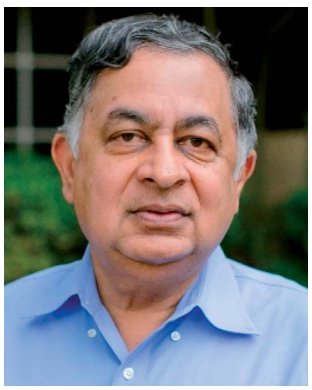

Arunava Gupta is a Distinguished University Research Professor at the University of Alabama (UA) with joint appointment in the Departments of Chemistry and Chemical Engineering. Gupta received his undergraduate degree from the Indian Institute of Technology, Kanpur, and Ph.D. degree in Chemical Physics from Stanford University. Prior to joining UA's faculty in 2004, he worked as a research staff member and manager at the IBM Thomas J. Watson Research Center in New York. Gupta's expertise is in investigating thin films and nanostructured materials for use in information technology and energy applications.

Strategies for synthesis

One of the attractive aspects of Cu-based chalcogenide nanocrystals is their size-controlled band gap and electronic energy levels. The composition and size of these semiconductor nanocrystals can be tailored to achieve desired optoelectronic properties for a wide range of major applications such as the absorber layer for solar cell devices, quantum dot light emitting diodes, and electrode materials for flexible supercapacitors (Fig. 1).[10] Therefore, there has been much research in recent years on the controlled synthesis of these multinary systems.[2,3,11,12] One of the challenges is to achieve the desired composition and crystal phase of these nanocrystals. Solution-based hot-injection and heat-up methods, single source precursor approaches, and the hydrothermal technique have been predominantly used for their synthesis. This section summarizes a few key synthetic perspectives from recent reports on Cu-based semiconductor nanocrystals (Fig. 2).

(a) Ternary systems

Ternary I–III–VI_2 nanocrystals, *i.e.* $CuInE_2$ (E: S, Se) have been synthesized in the chalcopyrite, wurtzite, and zinc blende phases, but it is difficult to structurally differentiate between the wurtzite and zinc blende products. These semiconductor nanocrystals exhibit direct and narrow band gaps. Balancing the reactivity of Cu and In through complexation of Cu^+ with a soft Lewis base like dodecanethiol (DDT) is an important

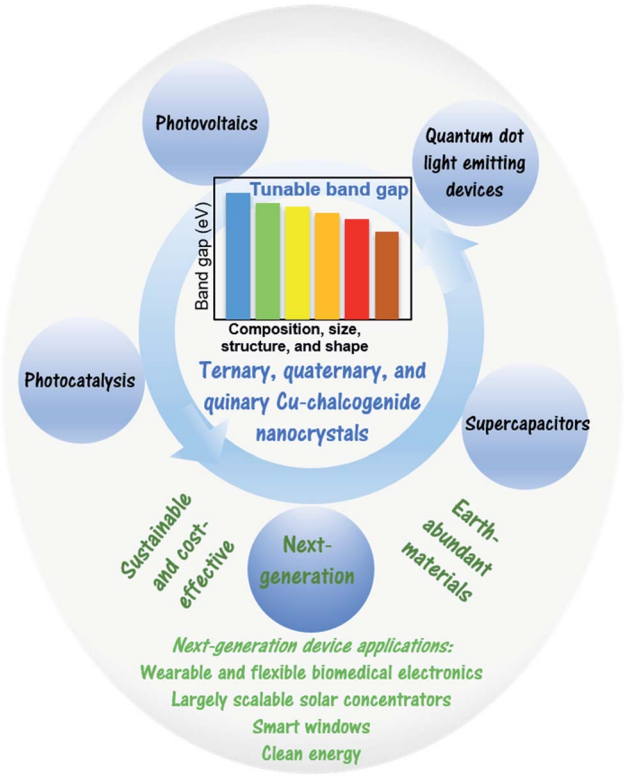

Fig. 1 Schematic presenting the advantages and different device applications of multinary Cu-chalcogenide nanocrystals.

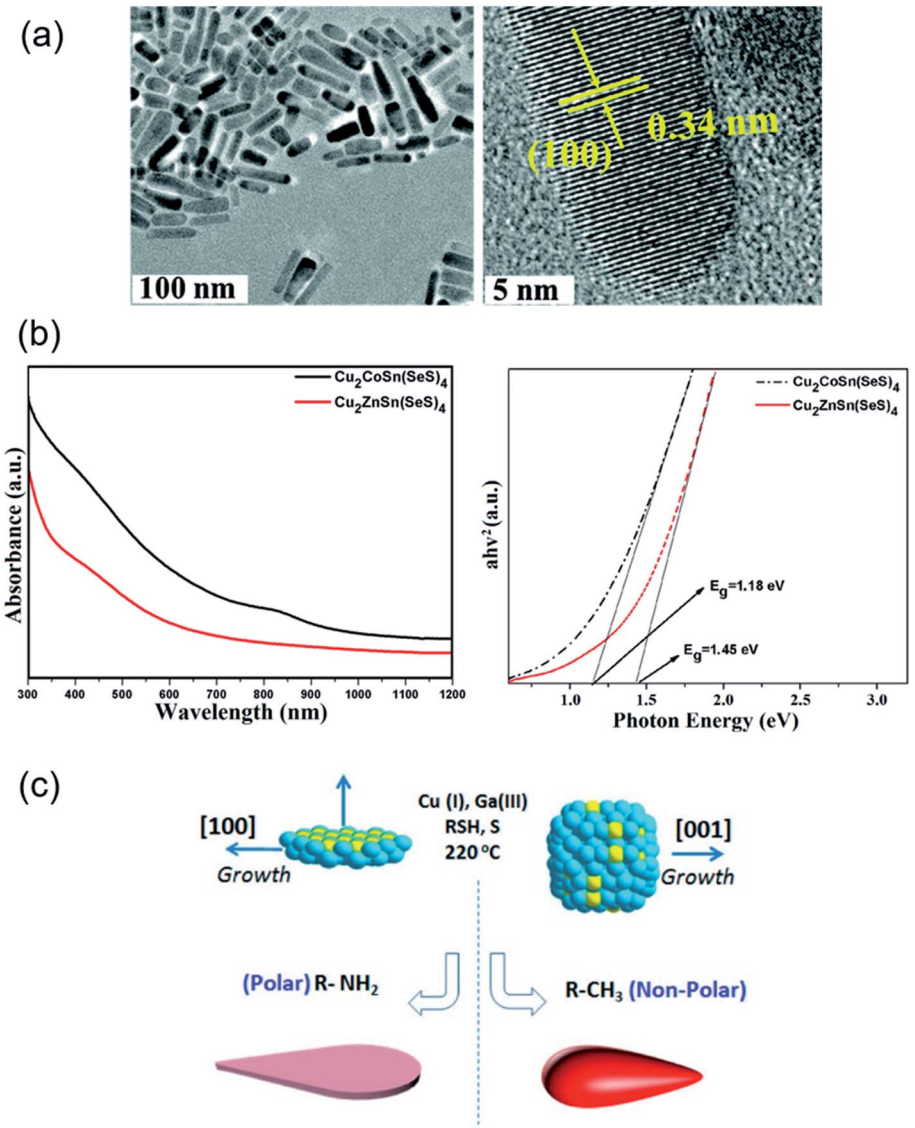

Fig. 2 Novel synthesis strategies for multinary Cu-chalcogenide nanocrystal compositions. (a) Transmission electron microscopy (TEM) and high-resolution TEM (HRTEM) images of wurtzite phase Cu_2ZnInS_{4-x} ($x = 0.5 \pm 0.3$) nanorods synthesized *via* a hot-injection technique. Reproduced with permission from ref. 63. Copyright: *Chem. Commun.*, The Royal Society of Chemistry; (b) ultra-violet visible absorption spectra and experimental Tauc plots of $Cu_2CoSn(SeS)_4$ and $Cu_2ZnSn(SeS)_4$ nanocrystals, Reproduced with permission from ref. 67. Copyright: *Sci. Rep.*, Nature; and (c) schematic showing the formation mechanism of two-dimensional tadpoles and tadpole-like $CuGaSe_2$ nanostructures. Reproduced with permission from ref. 35. Copyright: *Chem. Mater.*, ACS.

strategy to achieve the chalcopyrite phase of $CuInS_2$.[13–15] DDT plays the role of the sulfur source, ligand, and the solvent in these reactions. The optimum reaction temperature lies between 180 and 270 °C for this synthesis to obtain nanocrystal sizes within the quantum confinement regime. Larger $CuInS_2$ chalcopyrite nanocrystals of size 100 nm can be formed with thiourea as a sulfur source and alcohol solvents.[16,17] Elemental S and Se are also used as anionic sources for the synthesis of $CuInS_2$ and $CuInSe_2$ chalcopyrite nanocrystals.[18,19] This is particularly relevant for $CuInSe_2$ where elemental Se is used with oleylamine as the solvent and ligand to form smaller sized nanocrystals.[20,21] The use of ligands like trioctylphosphine, trioctylphosphine oxide or trioctylphosphine with Se powder instead of oleylamine promotes the growth of larger aggregated nanocrystals of $CuInSe_2$.[22–24] Alternately, the addition of a weaker binding ligand, dioctylphosphine oxide facilitates formation of anisotropic $CuInSe_2$ structures like nanowires. Other synthesis strategies for $CuInSe_2$ have also been reported with ethylenediamine as a substitute for oleylamine or the use of alkylthiols with Se powder to produce smaller nanocrystals of sizes 3–6 nm.[25,26]

The wurtzite phase of $CuInE_2$ is only stable in the nanocrystal form at room temperature. Alkylamine ligands in combination with DDT as the sulfur source play a major role in stabilizing this crystal phase.[27] Oleylamine or ligand mixtures of oleylamine/oleic acid and oleylamine/trioctyphosphine oxide are used with DDT to facilitate wurtzite phase ternary

nanocrystals. Metal acetates are common cationic precursors for wurtzite phase $CuInS_2$.[28–30] $CuInS_2$ wurtzite nanocrystals have also been synthesized with single source precursors such as $(Ph_3P)CuIn(SCPh)_4$ in the presence of trioctylphosphine oxide and DDT using reaction temperatures ranging from 150–250 °C.[31] Wurtzite phase $CuInSe_2$ nanocrystals can be obtained with diphenyldiselenide as the anionic precursor in oleylamine and copper oleate and $InCl_3$ as the precursors for the cations.[32,33] The formation mechanism of wurtzite phase $CuInE_2$ nanocrystals proceeds through the initial generation of nuclei of the corresponding binary complexes and growth of the ternary wurtzite nanocrystals in the presence of amines.[29,30] $CuInSe_2$ nanocrystals have also been reported *via* a cation exchange approach with anisotropic $Cu_{2-x}Se$ as the template and dodecaneselenol as the phosphine-free Se precursor.[34]

Das Adhikari *et al.* have reported the growth of anisotropic, tadpole-like $CuGaS_2$ nanocrystals using elemental S and alkyl thiols as dual sulfur sources with hexadecylamine ligand and metal acetylacetonate precursors and a mixture of octadecene and alkylamine as the solvent.[35] Elongated tadpole-like $CuGaS_2$ nanocrystals were also achieved in this synthesis by introducing zinc acetylacetonate in the reaction mixture. $CuGaS_2$ nanostructures were formed from seeds of Cu_2S nanodisks in these syntheses.

Our group has reported the first solution-based synthesis strategies for layered ternary $CuSbS_2$ with controlled thickness down to a monolayer.[36,37] These materials exhibit a band gap of 1.5 eV in the visible wavelength range and are highly promising for flexible supercapacitor and thin film solar cell applications. A bottom-up approach with elemental sulfur and oleylamine has been used for the formation of $CuSbS_2$ nanoplates with multiple layers. On the other hand, $CuSbS_2$ mesobelts have been synthesized *via* a hybrid bottom-up-and- top-down approach using 1-DDT and tertiary DDT (tert-DDT) as the sulfur source and an exfoliation strategy to form the controlled layered structure. Copper acetylacetonate and antimony chloride served as the metal precursors for both these syntheses. Ramasamy *et al.* have also reported a novel synthetic strategy to form all four p-type semiconductor phases of copper antimony sulphide for the first time.[38] The synthesis has been achieved with copper acetylacetonate and antimony chloride precursors in oleylamine and elemental S as the anionic precursor.

(b) Quaternary and pseudo-quaternary systems

Quaternary Cu-chalcogenide semiconductor nanocrystals offer a higher level of compositional flexibility to achieve tailored optical band gap and electronic energy levels compared to the ternary and binary complexes. At the same time, these materials are synthetically more challenging to achieve as multiple cations and chalcogen anions are incorporated within the crystal lattice of these systems.

$Cu(In_xGa_{1-x})Se_2$ and $Cu(In_xGa_{1-x})S_2$ (CIGS) nanocrystals have also been widely studied for their applications in photovoltaic devices. Alkylamines have been used as the capping agent in combination with Se powder as the anionic precursor for the syntheses of CIGS. The ligands play a major role in determining the final sizes of CIGS nanocrystals. For example, smaller-sized nanocrystals are formed with hexadecyl amine as compared to oleylamine.[39] The synthesis with hexadecyl amine proceeds through the formation of metal–ligand complexes, generation of various amorphous binary and ternary nanocrystal compositions and Se nanorods, which finally transform to the CIGS nanocrystals at higher temperatures. The use of single source precursors with ethanedithiol is suitable for the formation of ultra-small CIGS nanocrystals of sizes 2–3 nm.[40] DDT and tert-DDT have been used as the S source to achieve tunable tadpole-like and rod-like morphologies of the pure wurtzite phase CIGS nanocrystals.[41] Cation exchange has been a key synthetic strategy to overcome the limitation of precursors in direct synthesis for achieving multinary Cu-chalcogenide compositions.[42] In cation exchange, the miscibility of the parent compound and the product and the diffusion rate of cations to and from the nanocrystals are controlled through suitable reaction temperatures and concentrations of cations to achieve the desired nanocrystal composition. Recently, conversion of $CuInS_2$ to $CuGaInS_2$ nanocrystals has been achieved *via* the cation exchange of Cu^+ with Ga^{3+} mediated through $GaCl_3$-L (L: trioctylphosphine, triphenylphosphite, and diphenylphosphine) complexes.[42] Cu_2ZnSnS_4 (CZTS) and $Cu_2ZnSnSe_4$ (CZTSe) are the two most widely reported Cu-chalcogenide nanocrystals as they offer a promising and more sustainable platform as absorber layer materials for thin film solar cells.[43] The tetragonal kesterite phase is a common structure for these materials in the bulk, in which CuSn and CuZn exist as alternating layers in the direction of the crystal's *c*-axis. These materials can also exist in the stannite phase where SnZn and Cu form the alternate cation layers of the crystal structure. CZTS can be synthesized *via* injection of the sulfur source, elemental S, in oleylamine, into a hot solution of metal precursors in oleylamine.[44] A second method uses injection of both the elemental S in oleylamine and metal precursors into a hot solution of trioctylphosphine oxide.[45] This method facilitated excellent size control and formed CZTS nanocrystals in the size of 12 nm. Small CZTS nanocrystals of sizes between 2 and 7 nm have been synthesized using metal diethyldithiocarbamates with oleylamine.[46,47] Another strategy to form CZTS is *via* heat-up where the metal precursors and S source are mixed in oleylamine at room temperature prior to heating at the reaction temperature, 280 °C.[48] The amine ligand and solvent play a key role in the size-controlled synthesis of CZTS nanocrystals. For example, substitution of oleylamine with ethylenediamine forms aggregated particles or wire-like structures.[49,50] The use of thiourea as the anionic precursor in an ethylene glycol solvent has also yielded aggregated structures with sizes ranging from 100–500 nm.[51,52] The combination of ligand and S source has a strong influence on the phase of the final CZTS nanocrystals. An ethylenediamine ligand in a thiocarbamide sulfur precursor can stabilize the orthorhombic phase of the nanocrystals.[53] Alkylthiols as the stabilizing ligand facilitate the formation of wurtzite phase nanocrystals.[54,55] Singh *et al.* introduced the use of both DDT and tert-DDT in the presence of oleylamine to form elongated wurtzite phase nanocrystals of CZTS.[56] CZTS has also been synthesized *via* a novel chemical vapor deposition strategy using

diethyldithiocarbamate complexes of copper and zinc and alkyl derivatives of tin as the precursors.[57] On the other hand, CZTSSe nanocrystals of smaller sizes (20 nm) are synthesized *via* hot injection of trioctylphosphine selenide at 295 °C into a solution of metal chloride precursors in octadecene.[58] Liu *et al.* has also established a phosphine-free synthetic strategy for the formation of CZTSSe nanocrystals.[59] In this method, CZTSSe nanocrystals of size (3–4 nm) within the quantum confinement regime have been synthesized using hot injection of a solution of Se powder in DDT and oleylamine at 180 °C into a reaction mixture of metal chlorides in oleylamine and DDT. *In situ* cation exchange has also been applied for effective synthesis of CZTSSe nanoplatelets.[60] Recently, greener strategies like aqueous phase synthesis of size-controlled CZTS nanocrystals and CZTSSe have been reported.[61,62]

Recently, we have reported the synthesis of phase-pure wurtzite Cu_2ZnAS_{4-x} and $CuZn_2AS_4$ nanorods and nanoworms (A: Al, Ga, In; $0.1 \leq x \leq 0.5$).[63] A one-step hot-injection method using metal-acetylacetonate precursors, a combination of DDT and tert-DDT as anionic precursors, and oleylamine as the ligand and solvent has been applied to form these wurtzite nanocrystals. These nanocrystals can be further transformed to the stannite phase *via* annealing at high temperatures (400–500 °C). These materials show a composition-controlled direct band gap in the visible regime, which is attractive for photovoltaic applications. Our group has also reported the synthesis of oblate spheroid and triangular plate-shaped Cu_2FeSnS_4 (CFTS) nanocrystals with band gaps 1.54 and 1.46 eV, respectively using a similar solution-chemistry approach.[64] New quaternary $CuMSnS_4$ (M = In, Ga) nanocrystals have been synthesized in the wurtzite phase *via* a hot-injection method using a combination of n-DDT and t-DDT.[65] These nanocrystals exhibit strong visible light absorption, highly attractive for energy conversion applications.

Bera *et al.* have developed a thermodynamically controlled approach for the synthesis of a family of monodisperse $Cu_{12-x}M_xSb_4S_{13}$ (M = Zn^{II}, Cd^{II}, Mn^{II}, and Cu^{II}) tetrahedrite semiconductor nanostructures.[66] This has been achieved through prevention of cross-nucleation reactions with minimized reaction time in these syntheses.

(c) Quinary systems

Few reports are available on quinary Cu-chalcogenide systems due to the increased complexity in synthesis as compared to the quaternary and pseudo-quaternary compositions. *In situ* partial cation exchange has been used as a synthetic strategy for formation of plate-like copper zinc tin selenide-sulfide semiconductor nanocrystals.[60] Ozel *et al.* synthesized $Cu_2CoSn(SeS)_4$ and $Cu_2ZnSn(SeS)_4$ nanocrystals as catalysts for use as counter electrodes in dye-sensitized solar cells using a hot-injection approach.[67] A solution of metal precursors in the oleylamine ligand is heated to 280 °C, before injection of a solution of elemental S in oleylamine into the reaction mixture and heating at 280 °C for 30 min. These nanocrystals are 18–25 nm in size with a kesterite structure and optical band gaps of 1.18 eV and 1.45 eV. Recently, wurtzite phase $CuNi_xZn_{2-x}InS_4$ (x = 0–2) semiconductor nanocrystals have been reported with a tunable band gap in the visible range between 1.44 and 2.20 eV.[68] In this synthetic strategy, metal acetylacetonate precursors are heated to dissolution at 110 °C in oleic acid as the capping agent. DDT serves as the sulfur precursor and is quickly injected into the reaction mixture at 150 °C, followed by heating of the reactants at 210 °C. The formation mechanism of these nanocrystals

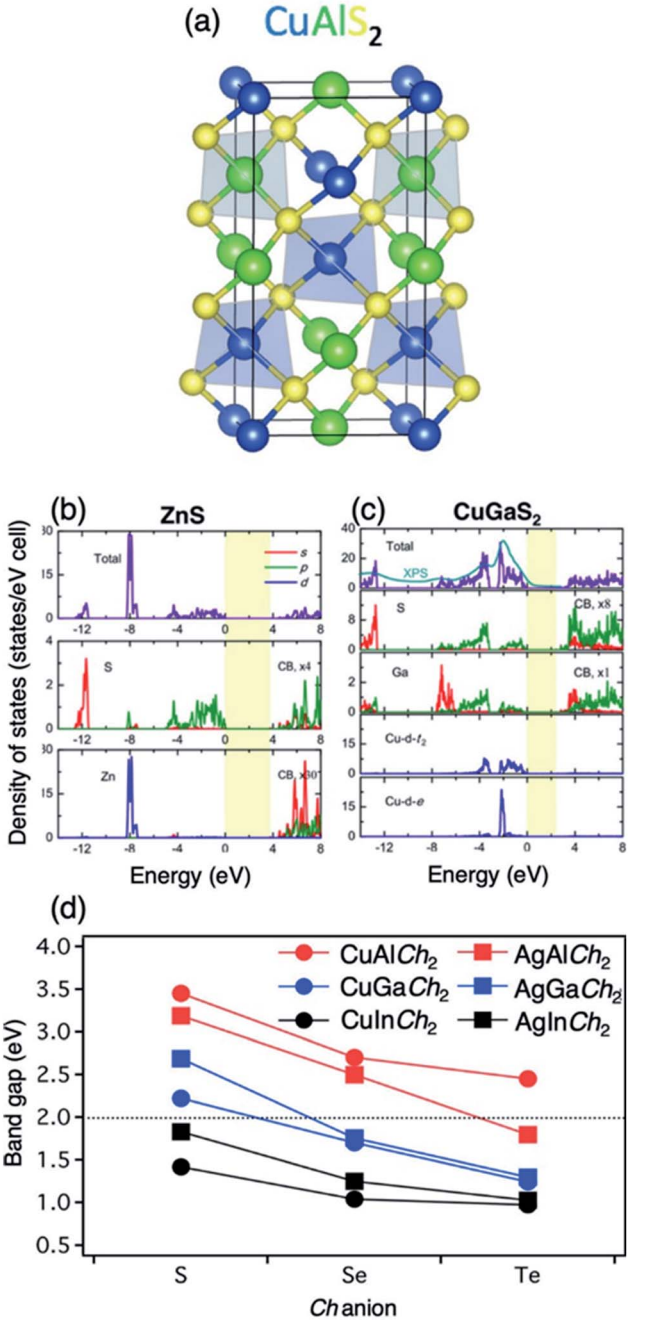

Fig. 3 Illustration of (a) the chalcopyrite structure, represented by $CuAlS_2$, and the DFT+U+G_0W_0 density of states from Zhang *et al.*[76] of (b) zinc blende ZnS compared to (c) chalcopyrite $CuGaS_2$, indicating p–d hybridization at the VBM in the chalcopyrite structure. Reproduced with permission from ref. 76 Copyright: *Comput. Mater. Sci.*, Elsevier, and (d) experimentally measured band gaps of I–III-Ch_2 semiconductors. Reproduced with permission from ref. 73. Copyright: *Chem. Rev.*, ACS.

proceeds through the initial generation of spherical $CuZn_2InS_4$ nanocrystals, which transform to the final bullet-shaped $CuNi_xZn_{2-x}InS_4$ nanocrystal product.

Emerging characterization techniques

Material characterization is an important component for bridging the path from synthesis of the new multicomponent Cu-chalcogenides to application. Transmission and scanning electron microscopy have been widely applied to investigate the size, morphology, and elemental composition of these nanocrystals. X-ray diffraction and X-ray photoelectron spectroscopy served as the golden standard to explore the crystal phase and oxidation state of the new nanocrystals. Grazing incidence small angle scattering and neutron scattering are also used to differentiate between two similar crystal phases. The experimental band gap of these nanostructures is typically measured using ultraviolet visible absorption spectroscopy and generation of Tauc plots. Recently, a few other characterization techniques have emerged that can be promising in predicting the unique properties of multicomponent chalcogenide nanocrystals.

(a) Hyperspectral infrared nanoimaging

Recently, hyperspectral infrared nanoimaging using nano-Fourier transform infrared spectroscopy (nano-FTIR) has been used in quantitative analysis of semiconductor samples and polymers (Fig. 4).[69,70] This technique is rapid and non-invasive and can serve as a platform for mapping the chemical distribution of cations and anions with a spatial resolution in multinary Cu-chalcogenide nanocrystals. The method is based on atomic force microscopy (AFM) principles, where the AFM tip concentrates the incident monochromatic or broadband infrared radiation field to a nanoscale spotsize at its apex. The scattered infrared field from the AFM tip is detected *via* an

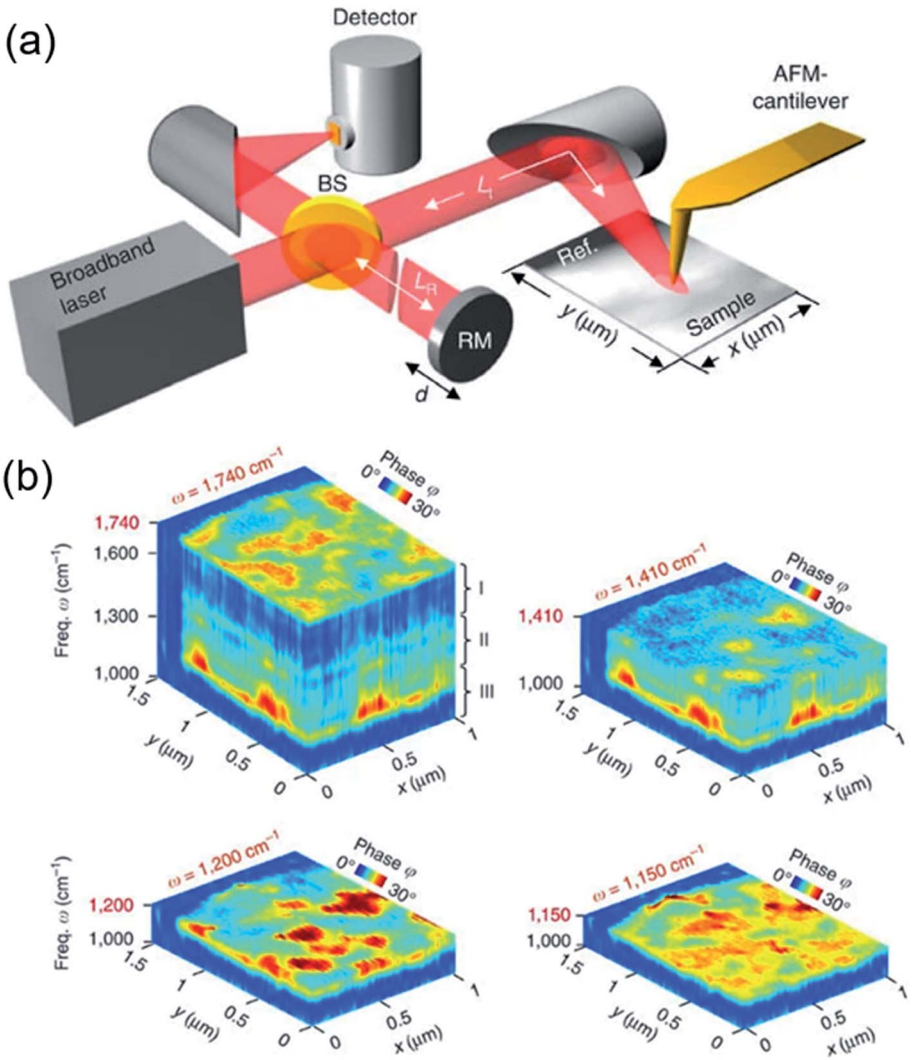

Fig. 4 Hyperspectral infrared nanoimaging. (a) Set-up of the instrument employing a mid-infrared laser continuum source for tip illumination and (b) hyperspectral infrared data cubes of a spectral resolution of 35 cm^{-1}, cut at different frequencies ω. They show the normalized phase ϕ of the tip-scattered light as a function of position (x, y) and frequency ω. Reproduced with permission from ref. 69. Copyright: *Nat. Commun.*, Nature.

interferometer to generate two-dimensional infrared amplitude and phase images of the sample. The possibility of mapping chemical distribution and interactions within the nanocrystals is much sought after from the perspective of multinary chalcogenide structures, and one that may be achieved through hyperspectral infrared nanoimaging.

(b) Thermogravimetric analysis

Thermogravimetric analysis (TGA) offers key information about the weight fraction and composition of the surface stabilizers on nanocrystals. Riedinger *et al.* used *in situ* TGA analysis during a solvent-free synthesis of CdSe nanocrystals to identify reactive organo-chalcogenide intermediate complexes.[71] These complexes have facilitated the molecular design of new precursor materials for CdSe nanocrystals. A similar TGA-based approach may be suitable in identification and molecular design of new precursor complexes for the multinary Cu-chalcogenide nanocrystals.

(c) Computational band gap predictions

Computational methods can be used to predict the band gap and absorption band edge of chalcogenide semiconductors. Several studies have applied density functional theory (DFT) calculations to determine the band gap (E_g) of new materials.[63,72] DFT is a fast and effective strategy for calculating the minimum energy gap between the valence band maxima and conduction band minima, but the method compromises the accuracy of band gap calculations for better computational efficiency. In some cases, these calculations may lead to underestimation of band gaps unless the parameters are empirically adjusted. Therefore, more computationally expensive methods like HSE06, many body perturbation theory (GW), and GW with the Beth–Salpeter equation (GW-BSE) are being investigated for band gap estimation of chalcogenide semiconductors on a case-by-case basis (Fig. 3).[73–76]

Applications

(a) Photovoltaics

The global energy demand is expected to reach 28 TW by 2050 with the increasing global population. This poses a burden on the finite fossil fuel energy sources. There is a growing demand for sustainable and cleaner energy and in 2017 solar photovoltaics (PV) have constituted 1.8% of the world's electricity with nearly 98 GW of new installations.[77,78] Silicon is the dominant material for PV devices with the highest recorded energy conversion efficiency of 26.7% using the heterojunction technology.[79] However, Si has an indirect band gap and the contacts in Si-based devices are made of Ag, which is found in limited quantities in the earth.[80] CdTe, CIGS, and CIGSe are the other most dominant absorber layer materials for thin-film solar cells, with CIGSe showing nearly 22.6% efficiency.[4,80–86] However, the limited availability and toxicity of these materials as well as the increased thickness of the device are some areas of improvement.[87] To this end, there have been several investigations in the past decade on quaternary CZTS solar cells. They are composed of cost-effective and easily available elements, but the highest efficiency of the kesterite phase CZTS and CZTSSe devices reached 9.2% and 12.6%, respectively.[5,88–92] There is further room for improvement because the thin film PV devices using viable materials and new earth-abundant multinary Cu-chalcogenides (*e.g.*, Cu_2FeSnS_4 (CFTS), Cu_2MnSnS_4 (CMTS), Cu_2BaSnS_4 and $Cu_2BaSn(S,Se)_4$ (CBTS and CBTSSe), Cu_2NiSnS_4 (CNTS), and Cu_2CoSnS_4) are currently being investigated for PV applications.[83,93] All these multinary Cu-chalcogenides show a suitable absorption coefficient ($>10^4$ cm^{-1}) and a band gap within the visible light range.[81] A key research thrust for these viable PV materials is to achieve better conversion efficiencies.

The p-type CFTS, being cheap and having a suitable band gap,[64] has been prepared as an absorber layer for thin film solar cells using cost-effective non-vacuum approaches. The best efficiency (*e.g.*, 2.95%) for CFTS has been reported with CFTS/Bi_2S_3 heterojunctions prepared *via* the SILAR method.[94] The SILAR technique for CFTS thin films was first reported by Guan *et al.*[95] Meng *et al.* fabricated CFTS solar cells with 0.11% efficiency *via* a sputtering approach.[96] CFTS thin films have been reported through several synthesis techniques such as electrostatic field assisted spray pyrolysis, aerosol assisted chemical vapor deposition, doctor blade deposition, and electrochemical deposition.[97–100] CMTS is another cost-effective p-type semiconductor that has been investigated in recent years as an absorber layer for thin film solar cells. CMTS thin films have been deposited on glass substrates *via* chemical routes.[101,102] These are most commonly found in the stannite phase. Direct liquid coating and annealing under a N_2 atmosphere has also been employed for preparation of CMTS thin films. These films showed an efficiency of 0.49%.[103] One of the highest efficiencies for CMTS PV devices (*i.e.*, 0.73%) has been achieved using Na doping between the CMTS layers *via* a spray technique to enhance grain growth.[104] In addition, the annealing conditions have a major influence in further enhancing the efficiency (*e.g.*, 0.83%) of CMTS solar cells.[105,106] There are currently a few literature reports on CNTS thin film solar cells and most of the studies have employed non-vacuum techniques like electrodeposition, spraying, and direct liquid coating.[107–110] Some of the limiting factors in increasing the efficiency of CZTS solar cells are the Cu-on-Zn and Zn-on-Cu antisite disorders.[111] CBTS does not exhibit these cation–cation antisite disorders and is a promising candidate for achieving higher efficiencies in thin film solar cells.[112] The CBTS and CBTSSe thin films have been prepared *via* vacuum deposition techniques in the few recent reports available on this material.[113] An efficiency of 5.2% has been obtained with a CBTSSe-based PV device.[114] Se substitution, band gap engineering, and post annealing in air have been used as strategies to enhance the performance of CBTS/CBTSSe thin film solar cells. Our group and others have investigated CCdTS/CCdTSSe nanocrystals and thin films for PV devices as Cd minimizes the detrimental ZnCu antisite defects.[115–117] A maximum efficiency of 3.1% has been achieved with these materials.[118] New multicomponent Cu-chalcogenides continue to be explored for higher efficiencies, cost-effectiveness, and viable alternatives for PV applications.

(b) Photocatalysis

Photocatalysis is an important scheme for clean energy production and environmental remediation.[119,120] The two major applications of photocatalysis are in hydrogen fuel generation through water-splitting reaction using sunlight and in the degradation of pollutant dyes for wastewater remediation.[121–123] TiO_2 nanoparticles have been traditionally used as photocatalysts for these reactions, but the wide band gap of the metal oxide based materials allows absorption of a small fraction of the solar spectrum within the ultraviolet region. Multinary chalcogenide nanocrystals are some of the most promising semiconductor photocatalysts with a suitable band gap for absorption in the visible light range.

To this end, ternary $CuInS_2$/ZnS nanorods have shown significant efficiency in H_2 generation from an aqueous solution containing S^{2-} and SO_3^{2-} as sacrificial reducing agents.[124] The H_2 production rate has been further increased in this reaction through addition of stable cocatalysts like Pt and Pd_4S nanocrystals on the surface of $CuInS_2$/ZnS nanorods. Another report established the high photocatalytic activity of alloyed $Zn_{1.6}Cu_{0.2}In_{0.2}S_2$ (ZCIS) microspheres for H_2 generation with a 15.45% quantum yield at 420 nm under Ru-loading.[125] This study also proved that smaller crystallite size of the semiconductor photocatalysts plays a key role in enhancing H_2 production. Qian *et al.* have shown the effect of semiconductor nanocrystal composition on photocatalytic H_2 generation rates using different compositions of ZCIS nanocrystals of 10 nm in size.[126] The $Zn_{1.6}Cu_{0.2}In_{0.2}S_2$ nanocrystal, showing a H_2 production rate of 984 μmol g^{-1} h^{-1} without any cocatalysts is the most favorable composition in this case too. This exceptional photocatalytic behavior of $Zn_{1.6}Cu_{0.2}In_{0.2}S_2$ semiconductor nanocrystals is attributed to the combined effect of a suitable band structure and excellent charge separation ability of these nanocrystals. Similar investigations of the effect of alloy compositions on photocatalytic H_2 yield have been conducted with the quaternary $Cu(In_xGa_{1-x})S_2$ chalcogenide nanorods.[127] It has been observed that there is an optimum level for substitution of In with Ga in these nanocrystal systems to achieve the maximum H_2 yield. The highest H_2 evolution has been obtained with the $CuIn_{0.3}Ga_{0.7}S_2$ compositions. Substitution of In with Ga raises the conduction band of the CIGS semiconductor nanocrystals and facilitates increased density of photogenerated electrons for enhanced reduction of H_2O to H_2. However, increasing the Ga concentration beyond the optimal limit induces wider band gaps that are unfavorable for photon absorption and photogenerated charge carrier density. The quaternary composition, CZTS has shown promising results for H_2 evolution in the presence of cocatalysts (*e.g.*, Au and Pt) that can induce enhanced separation of the charge carriers.[128–130] The crystal phase of the CZTS nanocrystals plays a strong role in the photocatalytic activity.[130] For example, the kesterite phase of CZTS is known to show a higher H_2 evolution rate than the wurtzite phase. The kesterite phase, formed through thermal annealing of the wurtzite nanocrystals, has a higher crystallinity and fewer defects than the wurtzite phase. This can likely account for enhanced photocatalytic behavior of the kesterite phase as defects act as recombination sites for the charge carriers and reduce the overall photocatalytic activity.

Visible light-driven photocatalysis is an effective and environment-friendly approach to render the non-biodegradable industrial dyes (*e.g.*, rhodamine B (RhB) and methylene blue) less toxic *via* degradation prior to release. RhB, a commonly used dye has been shown to degrade significantly by 91% within 2 h in the presence of ZCIS nanorods.[124] The degradation can be easily measured through time-dependent absorption spectra of the dye showing its marked decrease in concentration. In case of the ZnS-coated ZCIS nanorods, the RhB chromophore degraded completely *via* the formation of N-deethylated intermediates.[131] Other ternary and quaternary Cu-chalcogenide nanocrystals (*e.g.*, CZTS, $CuGaS_2$, and Cu_2ZnGeS_4) have also been effective in the degradation of dyes, but at a slower rate compared to the ZCIS nanorods.[132–134] CZTS nanocrystals coupled with Au or Pt metals show a higher photocatalytic activity for dye degradation compared to the unmodified CZTS nanocrystals.[128] The ternary $CuInSe_2$ and $CuInS_2$ chalcogenide nanocrystals have been known to serve as sensitizing agents for TiO_2 and ZnO platforms for photocatalytic degradation of dyes.[135,136]

(c) Quantum dot light emitting diodes

The advantage of quantum dot light emitting devices (QLEDs) over devices based on organic, polymeric, and inorganic materials is a combination of transformative color purity and brightness, lower turn-on voltage (<2 V), and an ultrathin active layer that facilitates device flexibility in the QLEDs.[25,137,138] A typical QLED consists of an anode, an electron transport material (ETM), a nanocrystal active layer, a hole transport material (HTM), and a cathode. Charge carriers from the respective charge transport layers (CTL) undergo radiative recombination in the nanocrystal active layer to generate the characteristic electroluminescence of the device. Currently, the visible light devices rely on Cd-chalcogenides and the Pb-chalcogenides predominate the near-infrared applications. In comparison, the Cu-based chalcogenides are composed of earth-abundant materials and provide a more sustainable platform for QLED applications. The multinary transition metal Cu-chalcogenide nanocrystals can be most attractive active layer materials for QLEDs due to their composition, size, and defect-dependent spectral emission.[2,6,139,140] The high energy states of the Cu 3d orbitals allow hybridization with the de-localized chalcogen-p orbitals.[6] This strong p-d hybridization and the comparable size and electronegativity between the transition metal cations and the chalcogens facilitate a large adjustable range of optoelectronic properties in these compounds. The defect concentrations and the possibility of non-stoichiometric and antisite defects in the Cu-chalcogenides can be used to further tailor the spectral and electroluminescence properties of these compounds.[141–143] The multinary Cu-chalcogenides exhibit size-dependent donor–acceptor pair recombination related photoluminescence properties. Several ZnS-shelled ternary and quaternary Cu-chalcogenide nanocrystal platforms like Mn doped CuInZnS,[144] $CuInS_2$/ZnS,[145–148] $CuInSe_2$/ZnS,[25]

CuInZnS/ZnS,[149] CuInGaS/ZnS,[150] and mixed systems of $CuInS_2$/ZnS and ZnCdSe/ZnS[143] have been promising for this type of QLED devices.[141] The current goals from a device performance perspective are to achieve miniaturization and structural flexibility, prevent loss of charge carriers and non-radiative recombination, and facilitate effective recombination of charge carriers within the emissive layer. To this end, a dominant trend in these Cu-chalcogenide nanocrystal systems is to increase quantum efficiency and resistance to photobleaching through synthetic control. For example, the molar ratio of Cu : In is adjusted in the CuInS-based systems to achieve better electroluminescence properties.

Another emerging and less explored application of semiconductor nanocrystals is in quantum dot white light emitting diodes (WLEDs). The WLEDs are currently aimed at achieving emissions comparable to a blackbody and are therefore highly useful as a large area lighting source, sunlight simulator, and as backlight sources for displays. WLEDs are more environment-friendly and consume less energy compared to the conventional light sources. The nanocrystal-based WLED devices started with a blue or UV light source being coupled with a small band gap down-conversion active material layer.[151–153] However, they have suffered from low external quantum efficiency (EQE) due to reabsorption of high-energy photons by the NCs, photobleaching, and non-uniform distribution of charge carriers. Broader emission spectra of the conventional light sources is also a disadvantage for these WLEDs. Therefore, the next class of devices, pioneered by Bawendi and Bulovic has been designed with a mixture of different light emitting nanocrystals to form electroluminescence-based WLEDs with higher color rendering index (CRI) and color purity.[154–156] The emission spectrum in these WLEDs can be precisely optimized with the appropriate ratio of red, green, and blue (RGB) emitting nanocrystals.[154,157,158] However, the wide gap in bandwidth between the various emitters is a limitation and adversely affects the color purity of the device. It has been later discovered that increasing the number of different types of emitter NCs (*e.g.*, blue, cyan, yellow, and red) can significantly improve the CRI. Recent technological advances in WLED have also shown a huge impact of ETM and HTM on the device performance (Fig. 5).[147,159,160] So far, ZnO nanocrystals have shown excellent charge mobility as the ETM and hybrid polymeric layers have been widely used as the HTM in WLED fabrication. The Cd-based materials (*e.g.*, CdSe–CdS core–shell nanocrystals) dominate the WLED applications, but more viable alternatives are currently being sought.[6,161,162] Materials that can increase the device lifetime are being investigated to further enhance and transform the WLED technology. Cu-based chalcogenides are a suitable candidate for WLEDs due to their inherent broad emission range.[163] The emission spectra can be further broadened through addition of dopants like Mn, Sn, and Ga in the Cu-chalcogenide nanocrystal structures.[144,145,164,165] To this end, multiple Cu-chalcogenide compositions have been successfully applied in WLEDs. For example, multinary Cu–Sn–In–S, $CuInS_2$,

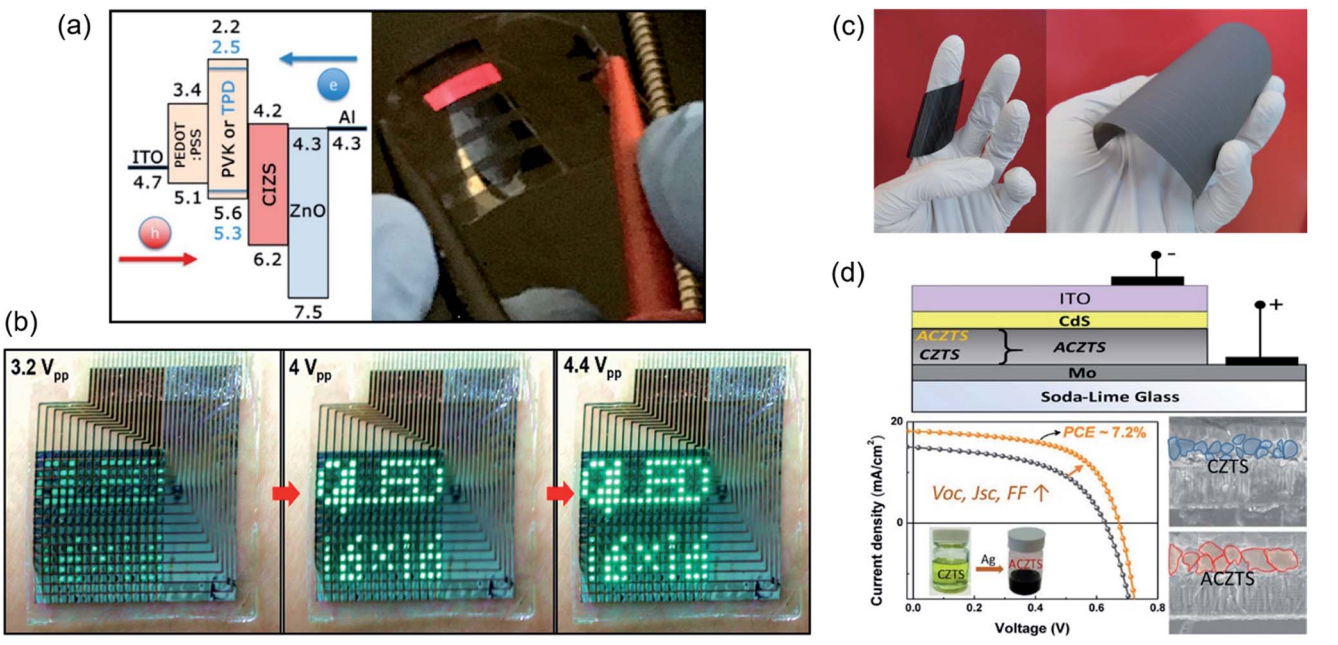

Fig. 5 Energy conversion and energy harvesting applications of multi-component Cu-chalcogenide nanocrystals. (a) Red-emitting QLEDs fabricated using $CuInS_2$–ZnS nanocrystals and two different HTMs (polyvinylcarbazole and poly(4-butylphenyldiphenylamine)). Reproduced with permission from ref. 147. Copyright: *ACS Appl. Mater. and Interfaces*, ACS; (b) ultra-thin QLED display in a wearable device showing sequential images at different operating voltages. Figure reproduced with permission from ref. 138. Copyright: *Adv. Mater.*, Wiley; (c) photo of highly flexible CIGS modules on two different substrates, (left) polyimide substrate showing strong curling behavior and (right) a steel substrate with lower curling behavior. Reproduced with permission from ref. 86. Copyright: *Engineering*, Elsevier; and (d) incorporation of Ag reduces the antisite defects and improves the grain size of kesterite-phase CZTS, facilitating an enhancement in open-circuit voltage and efficiency of the thin film solar cell. Reproduced with permission from ref. 5. Copyright: *ACS Energy Lett.*, ACS.

and Mn-doped Cu–In–Zn–S nanocrystals have been promising for electroluminescence type WLEDs.[143–145,166] Cu-chalcogenides have also been applied in WLEDs using down-conversion technology where the blue or UV-light is partially or fully converted to visible light.[165,167–173] The CIS/ZnS semiconductor nanocrystals and ZCIS alloy nanocrystals are most commonly used in down-conversion WLEDs.[174] Recently, Liu *et al.* have reported a new WLED composed of highly luminescent Cu–In–Zn–S nanocrystals showing a nearly 90% photoluminescence quantum yield.[175]

(d) Supercapacitors

Supercapacitors are an important class of sustainable energy storage devices due to their inherently high power density, longevity, and rapid charge/discharge capacity. Ternary and quaternary Cu-chalcogenide nanocrystals have served as attractive electrode materials for pseudocapacitive and electric double layer supercapacitors in recent studies.[176,177] For example, hydrothermally synthesized CFTS nanocrystals have exhibited excellent electrical double layer capacitor characteristics and unique photo-enhanced supercapacitive behavior.[178] The charge–discharge time and hence capacitance of these materials increase upon light irradiation. Our group has reported the promising specific supercapacitance and high cycling stability of layered copper antimony chalcogenide mesocrystals.[37,179] These electrodes have shown no loss of capacitance in cyclic voltammetry (CV) measurements even after 1000 cycles using different alkali metal ion electrolytes (*e.g.*, LiOH, NaOH, and KOH). In fact, the materials exhibit an improvement in charge-storage capacity after 200 cycles. Recently, ternary Cu_3SbS_4 and Cu_3MoS_4 grown on Ni foam have served as excellent binder-free electrodes for asymmetric supercapacitors.[180] These materials achieved the desirable combination of a high specific device capacitance of 213.6 F g^{-1}, excellent energy (58.15 W h kg^{-1}) density, better life-cycle, and maximum power density (6363.63 W kg^{-1}) for supercapacitor device applications.

(e) Luminescent solar concentrators

Luminescent solar concentrators are unique antenna-like structures to harvest and concentrate solar energy through a combination of photon absorption, luminescence, and waveguiding. The resulting high irradiance and narrowband output light is highly beneficial for solar energy conversion devices. In a simplest luminescent solar concentrator, a substrate of polymer or glass acts as a waveguide platform with the luminophores either embedded or coated on top. These devices are characterized through a combination of geometrical concentration factors and optical efficiency as performance indicators. Luminophore reabsorption losses remain the major limiting factors and possible areas of improvement for future large-scale luminescent solar concentrator technologies. To this end, semiconductor chalcogenide nanocrystals can be excellent candidates as spectral conversion phosphors for large scale luminescent solar concentrators.[181] Tunable properties and solution based processing approaches of the nanocrystals enable new engineered materials and cheaper fabrication methods for the luminescent solar concentrators. Doped nanocrystals such as $Cd_{1-x}Cu_xSe$ have been promising in minimizing reabsorption losses.[182] Meinardi *et al.*, used $CuInSe_xS_{2-x}$ nanocrystals embedded in photopolymerized poly(lauryl methacrylate) to realize materials that exhibit no distortion to perceived colors.[183] These materials are attractive for the photovoltaic window technology. These nanocrystals minimize the reabsorption mechanisms and can therefore, realize a high optical power efficiency of 3.2%. It has been shown that clustering of nanocrystals in the polymer matrix is a possible cause of limiting optical efficiency in large geometries due to light scattering losses.[184] Optimizing the nanocrystal concentrations can be the key to overcome light scattering losses. Sumner *et al.* realized optical power efficiencies up to 5.7% using an optimized concentration of $CuInS_2$/CdS nanocrystal phosphors. Recently, Liu *et al.* have reported heavy metal free luminophores for liquid solar concentrators using Cu-doped ZnInSe nanocrystals.[185] The materials have exhibited an optical efficiency of more than 3.5%, which is two times higher than polymer-based liquid solar concentrators. The highest recorded optical efficiency to date has been reported using high quantum yield (>90%), near-infrared emitting $CuInS_2$/ZnS nanocrystals in a polymer interlayer between glass substrates.[186] These laminated glass luminescent solar concentrators have shown an optical efficiency of 8.1% with nearly 44% transmission of visible light, which is highly attractive for windows. While luminescent solar concentrators have traditionally been used to harvest sunlight for photovoltaic devices recent progress has shown the application of $CuInSe_xS_{2-x}$/ZnS chalcogenide nanocrystals in novel optical fibre technology, broadband light sources for medical diagnostics, spectral conversion and light-guided agricultural devices, and large-area broadband detectors for telecommunications.[187]

Future perspective

In this review, we have summarized the recent advances made in the synthetic strategies, characterization techniques, and device applications for multinary Cu-chalcogenide semiconductor nanocrystals. The Cu-chalcogenide nanocrystals are less toxic compared to their Cd and Pb-based counterparts and are composed of more sustainable and earth-abundant elements. Recent progress in the synthesis of multinary chalcogenide compositions offer a wider spectrum of structural and compositional flexibility to achieve more tailored properties with the nanocrystals. This opens a wide scope of possibilities for next-generation devices. The multinary Cu-chalcogenides can catalyze new innovations in the field of wearable and flexible biomedical electronics.[188] For example, flexible QLEDs using multinary nanocrystals can be interfaced with sensors, resistive random access memory devices, and Bluetooth units to realize touch-sensitive displays, wearable biosensors for measuring heart-rate or motion detection, portable touch sensors for self-monitoring vital signs, and smart glasses to enhance perception of real-time images. The multinary Cu-chalcogenides can also be used as largely scalable

luminescent solar concentrator materials for energy-harvesting smart windows.[184] At the same time, these novel compositions can pave the way to high-throughput photovoltaic devices and higher efficiency photocatalytic reactions towards a more sustainable and cleaner conversion and harvesting of energy.

Conflicts of interest

There are no conflicts to declare.

Acknowledgements

SP thanks the National Science Foundation (NSF) for the funding and support provided through the NSF REU Award #1852042. AG thanks the NSF for the funding and support provided through Grant No. CHE-1508259.

References

1 O. Yarema, M. Yarema and V. Wood, *Chem. Mater.*, 2018, **30**, 1446.
2 C. Coughlan, M. Ibanez, O. Dobrozhan, A. Singh, A. Cabot and K. M. Ryan, *Chem. Rev.*, 2017, **117**, 5865.
3 O. Stroyuk, A. Raevskaya and N. Gaponik, *Chem. Soc. Rev.*, 2018, **47**, 5354.
4 T. Feurer, P. Reinhard, E. Avancini, B. Bissig, J. Lockinger, P. Fuchs, R. Carron, T. P. Weiss, J. Perrenoud, S. Stutterheim, S. Buecheler and A. Tiwari, *Prog. Photovoltaics*, 2017, **25**, 645.
5 A. Guchhait, Z. Su, Y. Tay, S. Shukla, W. Li, S. Leow, J. Tan, S. Lie, O. Gunawan and L. Wong, *ACS Energy Lett.*, 2016, **1**, 1256.
6 K. Knowles, K. Hartstein, T. Kilburn, A. Marchioro, H. Nelson, P. Whitham and D. Gamelin, *Chem. Rev.*, 2016, **116**, 10820.
7 S. Chen, X. Gong, A. Walsh and S. Wei, *Phys. Rev. B: Condens. Matter Mater. Phys.*, 2009, **79**, 165211.
8 Y. Chen, X. Feng, M. Liu, J. Su and S. Shen, *Nanophotonics*, 2016, **5**, 524.
9 J. Chang and E. R. Waclawik, *RSC Adv.*, 2014, **4**, 23505.
10 P. Matthews, P. McNaughter, D. Lewis and P. O'Brien, *Chem. Sci.*, 2017, **8**, 4177.
11 D. Aldakov, A. Lefrancois and P. Reiss, *J. Mater. Chem. C*, 2013, **1**, 3756.
12 D. Moodelly, P. Kowalik, P. Bujak, A. Pron and P. Reiss, *J. Mater. Chem. C*, 2019, **7**, 11665.
13 X. Tang, W. Cheng, E. Choo and J. Xue, *Chem. Commun.*, 2011, **47**, 5217.
14 M. Gromova, A. Lefrancois, L. Vaure, F. Agnese, D. Aldakov, A. Maurice, D. Djurado, C. Lebrun, A. de Geyer, T. Schulli, S. Pouget and P. Reiss, *J. Am. Chem. Soc.*, 2017, **139**, 15748.
15 L. Li, A. Pandey, D. Werder, B. Khanal, J. Pietryga and V. Klimov, *J. Am. Chem. Soc.*, 2011, **133**, 1176.
16 C. Yu, J. Yu, H. Wen and C. Zhang, *Mater. Lett.*, 2009, **63**, 1984.
17 K. Das, S. Panda, S. Gorai, P. Mishra and S. Chaudhuri, *Mater. Res. Bull.*, 2008, **43**, 2742.
18 A. Pein, M. Baghbanzadeh, T. Rath, W. Haas, E. Maier, H. Amenitsch, F. Hofer, C. Kappe and G. Trimmel, *Inorg. Chem.*, 2011, **50**, 193.
19 M. Chiang, S. Chang, C. Chen, F. Yuan and H. Tuan, *J. Phys. Chem. C*, 2011, **115**, 1592.
20 B. Koo, R. Patel and B. Korgel, *J. Am. Chem. Soc.*, 2009, **131**, 3134.
21 A. de Kergommeaux, A. Fiore, N. Bruyant, F. Chandezon, P. Reiss, A. Pron, R. de Bettignies and J. Faure-Vincent, *Sol. Energy Mater. Sol. Cells*, 2011, **95**, S39.
22 J. He, W. Zhou, M. Li, Z. Hou, Y. Du and S. Wu, *Mater. Lett.*, 2012, **66**, 96.
23 S. Wark, C. Hsia, Z. Luo and D. Son, *J. Mater. Chem.*, 2011, **21**, 11618.
24 A. Wooten, D. Werder, D. Williams, J. Casson and J. Hollingsworth, *J. Am. Chem. Soc.*, 2009, **131**, 16177.
25 H. Zhong, Z. Wang, E. Bovero, Z. Lu, F. van Veggel and G. Scholes, *J. Phys. Chem. C*, 2011, **115**, 12396.
26 H. Zhong, Y. Li, M. Ye, Z. Zhu, Y. Zhou, C. Yang and Y. Li, *Nanotechnology*, 2007, **18**, 025602.
27 D. Pan, L. An, Z. Sun, W. Hou, Y. Yang, Z. Yang and Y. Lu, *J. Am. Chem. Soc.*, 2008, **130**, 5620.
28 M. Kruszynska, H. Borchert, J. Parisi and J. Kolny-Olesiak, *J. Am. Chem. Soc.*, 2010, **132**, 15976.
29 S. Connor, C. Hsu, B. Weil, S. Aloni and Y. Cui, *J. Am. Chem. Soc.*, 2009, **131**, 4962.
30 X. Lu, Z. Zhuang, Q. Peng and Y. Li, *Crystengcomm*, 2011, **13**, 4039.
31 S. Batabyal, L. Tian, N. Venkatram, W. Ji and J. Vittal, *J. Phys. Chem. C*, 2009, **113**, 15037.
32 B. Tappan, G. Barim, J. Kwok and R. Brutchey, *Chem. Mater.*, 2018, **30**, 5704.
33 D. Houck and B. Korgel, *Chem. Mater.*, 2018, **30**, 8359.
34 A. Berends, W. van der Stam, Q. Akkerman, J. Meeldijk, J. van der Lit and C. Donega, *Chem. Mater.*, 2018, **30**, 3836.
35 S. Das Adhikari, A. Dutta, G. Prusty, P. Sahu and N. Pradhan, *Chem. Mater.*, 2017, **29**, 5384.
36 K. Ramasamy, H. Sims, W. Butler and A. Gupta, *J. Am. Chem. Soc.*, 2014, **136**, 1587.
37 K. Ramasamy, R. K. Gupta, S. Palchoudhury, S. Ivanov and A. Gupta, *Chem. Mater.*, 2014, **27**, 379.
38 K. Ramasamy, H. Sims, W. Butler and A. Gupta, *Chem. Mater.*, 2014, **26**, 2891.
39 M. Ahmadi, S. Pramana, L. Xi, C. Boothroyd, Y. Lam and S. Mhaisalkar, *J. Phys. Chem. C*, 2012, **116**, 8202.
40 C. Sun, J. Gardner, G. Long, C. Bhattacharya, A. Thurber, A. Punnoose, R. Rodriguez and J. Pak, *Chem. Mater.*, 2010, **22**, 2699.
41 A. Wang, X. Zhang, N. Bao, B. Lin and A. Gupta, *J. Am. Chem. Soc.*, 2011, **133**, 11072.
42 S. Hinterding, A. Berends, M. Kurttepeli, M. Moret, J. Meeldijk, S. Bals, W. van der Stam and C. Donega, *ACS Nano*, 2019, **13**, 12880.
43 K. Ramasamy, M. A. Malik and P. O'Brien, *Chem. Commun.*, 2012, **48**, 5703.
44 Q. Guo, H. Hillhouse and R. Agrawal, *J. Am. Chem. Soc.*, 2009, **131**, 11672.

45 S. Riha, B. Parkinson and A. Prieto, *J. Am. Chem. Soc.*, 2009, **131**, 12054.
46 A. Khare, A. W. Wills, L. Ammerman, D. Norris and E. Aydil, *Chem. Commun.*, 2011, **47**, 11721.
47 Y. Jung, J. Kim and J. Lee, *J. Am. Chem. Soc.*, 2010, **132**, 178.
48 C. Steinhagen, M. Panthani, V. Akhavan, B. Goodfellow, B. Koo and B. Korgel, *J. Am. Chem. Soc.*, 2009, **131**, 12554.
49 M. Cao and Y. Shen, *J. Cryst. Growth*, 2011, **318**, 1117.
50 L. Shi, C. Pei, Y. Xu and Q. Li, *J. Am. Chem. Soc.*, 2011, **133**, 10328.
51 O. Zaberca, F. Oftinger, J. Chane-Ching, L. Datas, A. Lafond, P. Puech, A. Balocchi, D. Lagarde and X. Marie, *Nanotechnology*, 2012, **23**, 185402.
52 Y. Zhou, W. Zhou, M. Li, Y. Du and S. Wu, *J. Phys. Chem. C*, 2011, **115**, 19632.
53 H. Jiang, P. Dai, Z. Feng, W. Fan and J. Zhan, *J. Mater. Chem.*, 2012, **22**, 7502.
54 M. Regulacio, C. Ye, S. Lim, M. Bosman, E. Ye, S. Chen, Q. Xu and M. Han, *Chem.–Eur. J.*, 2012, **18**, 3127.
55 X. Lu, Z. Zhuang, Q. Peng and Y. Li, *Chem. Commun.*, 2011, **47**, 3141.
56 A. Singh, H. Geaney, F. Laffir and K. Ryan, *J. Am. Chem. Soc.*, 2012, **134**, 2910.
57 K. Ramasamy, M. A. Malik and P. O'Brien, *Chem. Sci.*, 2011, **2**, 1170.
58 A. Shavel, J. Arbiol and A. Cabot, *J. Am. Chem. Soc.*, 2010, **132**, 4514.
59 Y. Liu, D. Yao, L. Shen, H. Zhang, X. Zhang and B. Yang, *J. Am. Chem. Soc.*, 2012, **134**, 7207.
60 V. Lesnyak, C. George, A. Genovese, M. Prato, A. Casu, S. Ayyappan, A. Scarpellini and L. Manna, *ACS Nano*, 2014, **8**, 8407.
61 O. Stroyuk, A. Raevskaya, O. Selyshchev, V. Dzhagan, N. Gaponik, D. Zahn and A. Eychmuller, *Sci. Rep.*, 2018, **8**, 13677.
62 C. Ritchie, A. Chesman, J. Jasieniak and P. Mulvaney, *Chem. Mater.*, 2019, **31**, 2138.
63 A. Ghosh, S. Palchoudhury, T. Rajalingam, Z. Zhou, N. Naghibolashrafi, K. Ramasamy and A. Gupta, *Chem. Commun.*, 2016, **52**, 264.
64 X. Zhang, N. Bao, K. Ramasamy, A. Wang, Y. Wang, B. Lin and A. Gupta, *Chem. Commun.*, 2012, **48**, 4956.
65 K. Ramasamy, P. Shinde, N. Naghibolashrafi, S. Pan and A. Gupta, *Chem. Commun.*, 2018, **54**, 11757.
66 S. Bera, A. Dutta, S. Mutyala, D. Ghosh and N. Pradhan, *J. Phys. Chem. Lett.*, 2018, **9**, 1907.
67 F. Ozel, A. Sarilmaz, B. Istanbullu, A. Aljabour, M. Kus and S. Sonmezoglu, *Sci. Rep.*, 2016, **6**, 29207.
68 Y. Xu, Q. Fu, S. Lei, L. Lai, J. Xiong, Q. Bian, Y. Xiao and B. Cheng, *J. Alloys Compd.*, 2020, **820**, 153436.
69 I. Amenabar, S. Poly, M. Goikoetxea, W. Nuansing, P. Lasch and R. Hillenbrand, *Nat. Commun.*, 2017, **8**, 14402.
70 N. Aghamiri, F. Huth, A. Huber, A. Fali, R. Hillenbrand and Y. Abate, *Opt. Express*, 2019, **27**, 24231.
71 A. Riedinger, A. Mule, P. Knusel, F. Ott, A. Rossinelli and D. Norris, *Chem. Commun.*, 2018, **54**, 11789.
72 A. Jain, S. Ong, G. Hautier, W. Chen, W. Richards, S. Dacek, S. Cholia, D. Gunter, D. Skinner, G. Ceder and K. Persson, *APL Mater.*, 2013, **1**, 011002.
73 R. Woods-Robinson, Y. Han, H. Zhang, T. Ablekim, I. Khan, K. Persson and A. Zakutayev, *Chem. Rev.*, 2020, **120**, 4007.
74 J. Zhou, B. Sumpter, P. Kent and J. Huang, *ACS Appl. Mater. Interfaces*, 2015, **7**, 1458.
75 W. Li, C. Walther, A. Kuc and T. Heine, *J. Chem. Theory Comput.*, 2013, **9**, 2950.
76 Y. Zhang, L. Xi, Y. Wang, J. Zhang, P. Zhang and W. Zhang, *Comput. Mater. Sci.*, 2015, **108**, 239.
77 M. Hoffert, K. Caldeira, A. Jain, E. Haites, L. Harvey, S. Potter, M. Schlesinger, S. Schneider, R. Watts, T. Wigley and D. Wuebbles, *Nature*, 1998, **395**, 881.
78 REN21, *Renewables Global Status Report*, Paris, 2018.
79 L. Andreani, A. Bozzola, P. Kowalczewski, M. Liscidini and L. Redorici, *Adv. Phys.: X*, 2019, **4**, 1548305.
80 C. Tao, J. Jiang and M. Tao, *Sol. Energy Mater. Sol. Cells*, 2011, **95**, 3176.
81 R. Manivannan and S. Victoria, *Sol. Energy*, 2018, **173**, 1144.
82 E. Peccerillo and K. Durose, *MRS Energy Sustain.*, 2018, **5**, E13.
83 A. Le Donne, V. Trifiletti and S. Binetti, *Front. Chem.*, 2019, **7**, 297.
84 P. Nayak, S. Mahesh, H. Snaith and D. Cahen, *Nat. Rev. Mater.*, 2019, **4**, 269.
85 P. Jackson, R. Wuerz, D. Hariskos, E. Lotter, W. Witte and M. Powalla, *Phys. Status Solidi RRL*, 2016, **10**, 583.
86 M. Powalla, S. Paetel, D. Hariskos, R. Wuerz, F. Kessler, P. Lechner, W. Wischmann and T. Friedlmeier, *Engineering*, 2017, **3**, 445.
87 H. Choi and S. Jeong, *International Journal of Precision Engineering and Manufacturing-Green Technology*, 2018, **5**, 349.
88 K. Sun, C. Yan, F. Liu, J. Huang, F. Zhou, J. Stride, M. Green and X. Hao, *Adv. Energy Mater.*, 2016, **6**, 1600046.
89 W. Wang, M. Winkler, O. Gunawan, T. Gokmen, T. Todorov, Y. Zhu and D. Mitzi, *Adv. Energy Mater.*, 2014, **4**, 1301465.
90 X. Liu, Y. Feng, H. Cui, F. Liu, X. Hao, G. Conibeer, D. Mitzi and D. M. Green, *Prog. Photovoltaics*, 2016, **24**, 879.
91 F. Jiang, C. Ozaki, Gunawan, T. Harada, Z. Tang, T. Minemoto, Y. Nose and S. Ikeda, *Chem. Mater.*, 2016, **28**, 3283.
92 D. Mitzi, O. Gunawan, T. Todorov, K. Wang and S. Guha, *Sol. Energy Mater. Sol. Cells*, 2011, **95**, 1421.
93 E. Wu, J. Jin, S. Liu, D. Li, S. Gao, F. Deng, X. Yan, Y. Xiong and H. Tang, *Sci. Rep.*, 2019, **9**, 12337.
94 S. Chatterjee and A. Pal, *Sol. Energy Mater. Sol. Cells*, 2017, **160**, 233.
95 H. Guan, H. Shen, B. Jiao and X. Wang, *Mater. Sci. Semicond. Process.*, 2014, **25**, 159.
96 X. Meng, H. Deng, J. He, L. Sun, P. Yang and J. Chu, *Mater. Lett.*, 2015, **151**, 61.
97 D. Khadka and J. Kim, *J. Alloys Compd.*, 2015, **638**, 103.
98 P. Kevin, M. A. Malik and P. O'Brien, *New J. Chem.*, 2015, **39**, 7046.

99 G. Chen, J. Li, S. Chen, Z. Huang, M. Wu, J. Zhao, W. Wang, H. Lin and C. Zhu, *Mater. Chem. Phys.*, 2017, **188**, 95.
100 X. Miao, R. Chen and W. Cheng, *Mater. Lett.*, 2017, **193**, 183.
101 J. Yu, H. Deng, J. Tao, L. Chen, H. Cao, L. Sun, P. Yang and J. Chu, *Mater. Lett.*, 2017, **191**, 186.
102 S. Marchionna, A. Le Donne, M. Merlini, S. Binetti, M. Acciarri and F. Cernuschi, *J. Alloys Compd.*, 2017, **693**, 95.
103 L. Chen, H. Deng, J. Tao, H. Cao, L. Huang, L. Sun, P. Yang and J. Chu, *RSC Adv.*, 2015, **5**, 84295.
104 R. Prabhakar, Z. Su, Z. Xin, T. Baikie, L. Woei, S. Shukla, S. Batabyal, O. Gunawan and L. Wong, *Sol. Energy Mater. Sol. Cells*, 2016, **157**, 867.
105 A. Le Donne, S. Marchionna, M. Acciarri, F. Cernuschi and S. Binetti, *Sol. Energy*, 2017, **149**, 125.
106 M. Neuschitzer, Y. Sanchez, T. Olar, T. Thersleff, S. Lopez-Marino, F. Oliva, M. Espindola-Rodriguez, H. Xie, M. Placidi, V. Izquierdo-Roca, I. Lauermann, K. Leifer, A. Perez-Rodriguez and E. Saucedo, *Chem. Mater.*, 2015, **27**, 5279.
107 N. Bitri, S. Dridi, F. Chaabouni and M. Abaab, *Mater. Lett.*, 2018, **213**, 31.
108 K. Mokurala, S. Mallick, P. Bhargava, S. Siol, T. Klein and M. van Hest, *J. Alloys Compd.*, 2017, **725**, 510.
109 S. Dridi, N. Bitri and M. Abaab, *Mater. Lett.*, 2017, **204**, 61.
110 C. Yang, Y. Chen, M. Lin, S. Wu, L. Li, W. Liu, X. Wu and F. Zhang, *Mater. Lett.*, 2016, **166**, 101.
111 T. Gokmen, O. Gunawan, T. Todorov and D. Mitzi, *Appl. Phys. Lett.*, 2013, **103**, 103506.
112 Z. Xiao, W. Meng, J. Li and Y. Yan, *ACS Energy Lett.*, 2017, **2**, 29.
113 J. Ge, Y. Yu and Y. Yan, *ACS Energy Lett.*, 2016, **1**, 583.
114 D. Shin, T. Zhu, X. Huang, O. Gunawan, V. Blum and D. Mitzi, *Adv. Mater.*, 2017, **29**, 1606945.
115 K. Ramasamy, X. Zhang, R. Bennett and A. Gupta, *RSC Adv.*, 2013, **3**, 1186.
116 S. Hussain, G. Murtaza, S. Khan, A. Khan, M. Ali, M. Faizan, A. Mahmood and R. Khenata, *Mater. Res. Bull.*, 2016, **79**, 73.
117 M. Rouchdi, E. Salmani, N. Hassanain and A. Mzerd, *Opt. Quantum Electron.*, 2017, **49**, 165.
118 W. Zhao, G. Wang, Q. Tian, L. Huang, S. Gao and D. Pan, *Sol. Energy Mater. Sol. Cells*, 2015, **133**, 15.
119 P. Moroz, A. Boddy and M. Zamkov, *Front. Chem.*, 2018, **6**, 353.
120 J. Corredor, M. Rivero, C. Rangel, F. Gloaguen and I. Ortiz, *J. Chem. Technol. Biotechnol.*, 2019, **94**, 3049.
121 C. Xu, P. Anusuyadevi, C. Aymonier, R. Luque and S. Marre, *Chem. Soc. Rev.*, 2019, **48**, 3868.
122 J. Luo, S. Zhang, M. Sun, L. Yang, S. Luo and J. Crittenden, *ACS Nano*, 2019, **13**, 9811.
123 F. Haque, T. Daeneke, K. Kalantar-zadeh and J. Ou, *Nano-Micro Lett.*, 2018, **10**, 23.
124 C. Ye, M. Regulacio, S. Lim, S. Li, Q. Xu and M. Han, *Chem.–Eur. J.*, 2015, **21**, 9514.
125 X. Zhang, Y. Du, Z. Zhou and L. Guo, *Int. J. Hydrogen Energy*, 2010, **35**, 3313.
126 M. Xu, J. Zai, Y. Yuan and X. Qian, *J. Mater. Chem.*, 2012, **22**, 23929.
127 X. Yu, X. An, A. Shavel, M. Ibanez and A. Cabot, *J. Mater. Chem. A*, 2014, **2**, 12317.
128 X. Yu, A. Shavel, X. An, Z. Luo, M. Ibanez and A. Cabot, *J. Am. Chem. Soc.*, 2014, **136**, 9236.
129 E. Ha, L. Lee, J. Wang, F. Li, K. Wong and S. Tsang, *Adv. Mater.*, 2014, **26**, 3496.
130 Z. Chang, W. Zhou, D. Kou, Z. Zhoua and S. Wu, *Chem. Commun.*, 2014, **50**, 12726.
131 W. Zhang and X. Zhong, *Inorg. Chem.*, 2011, **50**, 4065.
132 Q. Ren, W. Wang, H. Shi and Y. Liang, *Micro Nano Lett.*, 2014, **9**, 505.
133 M. Regulacio, C. Ye, S. Lim, Y. Zheng, Q. Xu and M. Han, *Crystengcomm*, 2013, **15**, 5214.
134 C. Fan, M. Regulacio, C. Ye, S. Lim, S. Lua, Q. Xu, Z. Dong, A. Xu and M. Han, *Nanoscale*, 2015, **7**, 3247.
135 Y. Liao, H. Zhang, Z. Zhong, L. Jia, F. Bai, J. Li, P. Zhong, H. Chen and J. Zhang, *ACS Appl. Mater. Interfaces*, 2013, **5**, 11022.
136 F. Shen, W. Que, Y. He, Y. Yuan, X. Yin and G. Wang, *ACS Appl. Mater. Interfaces*, 2012, **4**, 4087.
137 Y. Shirasaki, G. Supran, M. Bawendi and V. Bulovic, *Nat. Photonics*, 2013, **7**, 13.
138 J. Kim, H. Shim, J. Yang, M. Choi, D. Kim, T. Hyeon and D. Kim, *Adv. Mater.*, 2017, **29**, 1700217.
139 J. Yang, M. Choi, D. Kim and T. Hyeon, *Adv. Mater.*, 2016, **28**, 1176.
140 G. Supran, Y. Shirasaki, K. Song, J. Caruge, P. Kazlas, S. Coe-Sullivan, T. Andrew, M. Bawendi and V. Bulovic, *MRS Bull.*, 2013, **38**, 703.
141 X. Bai, F. Purcell-Milton and Y. Gun'ko, *Nanomaterials*, 2019, **9**, E85.
142 Q. Rice, S. Raut, R. Chib, Z. Gryczynski, I. Gryczynski, W. Zhang, X. Zhong, M. Abdel-Fattah, B. Tabibi and J. Seo, *J. Nanomater.*, 2014, **2014**, 979875.
143 S. Wepfer, J. Frohleiks, A. Hong, H. Jang, G. Bacher and E. Nannen, *ACS Appl. Mater. Interfaces*, 2017, **9**, 11224.
144 W. Zhang, C. Pan, F. Cao and X. Yang, *J. Mater. Chem. C*, 2017, **5**, 10533.
145 J. Chen, Y. Li, L. Wang, T. Zhou and R. Xie, *Nanoscale*, 2018, **10**, 9788.
146 B. Chen, H. Zhong, W. Zhang, Z. Tan, Y. Li, C. Yu, T. Zhai, Y. Bando, S. Yang and B. Zou, *Adv. Funct. Mater.*, 2012, **22**, 2081.
147 G. Zaiats, S. Ikeda, S. Kinge and P. Kamat, *ACS Appl. Mater. Interfaces*, 2017, **9**, 30741.
148 J. Kim and H. Yang, *Opt. Lett.*, 2014, **39**, 5002.
149 X. Yuan, J. Hua, R. Zeng, D. Zhu, W. Ji, P. Jing, X. Meng, J. Zhao and H. Li, *Nanotechnology*, 2014, **25**, 435202.
150 J. Kim, K. Lee, D. Jo, Y. Lee, J. Hwang and H. Yang, *Appl. Phys. Lett.*, 2014, **105**, 133104.
151 C. Ruan, Y. Zhang, M. Lu, C. Ji, C. Sun, X. Chen, H. Chen, V. Colvin and W. Yu, *Nanomaterials*, 2016, **6**, 13.
152 K. Gugula, L. Stegemann, P. Cywinski, C. Strassert and M. Bredol, *RSC Adv.*, 2016, **6**, 10086.

153 E. Jang, S. Jun, H. Jang, J. Llim, B. Kim and Y. Kim, *Adv. Mater.*, 2010, **22**, 3076.
154 P. Anikeeva, J. Halpert, M. Bawendi and V. Bulovic, *Nano Lett.*, 2007, **7**, 2196.
155 J. Caruge, J. Halpert, V. Wood, V. Bulovic and M. Bawendi, *Nat. Photonics*, 2008, **2**, 247.
156 K. Lee, C. Han, H. Kang, H. Ko, C. Lee, J. Lee, N. Myoung, S. Yim and H. Yang, *ACS Nano*, 2015, **9**, 10941.
157 T. Kim, D. Chung, J. Ku, I. Song, S. Sul, D. Kim, K. Cho, B. Choi, J. Kim, S. Hwang and K. Kim, *Nat. Commun.*, 2013, **4**, 2637.
158 K. Cho, E. Lee, W. Joo, E. Jang, T. Kim, S. Lee, S. Kwon, J. Han, B. Kim, B. Choi and J. Kim, *Nat. Photonics*, 2009, **3**, 341.
159 W. Cao, C. Xiang, Y. Yang, Q. Chen, L. Chen, X. Yan and L. Qian, *Nat. Commun.*, 2018, **9**, 2608.
160 J. Kwak, W. Bae, D. Lee, I. Park, J. Lim, M. Park, H. Cho, H. Woo, D. Yoon, K. Char, S. Lee and C. Lee, *Nano Lett.*, 2012, **12**, 2362.
161 B. Chen, N. Pradhan and H. Zhong, *J. Phys. Chem. Lett.*, 2018, **9**, 435.
162 Y. Jiang, S. Cho and M. Shim, *J. Mater. Chem. C*, 2018, **6**, 2618.
163 P. Whitham, K. Knowles, P. Reid and D. Gamelin, *Nano Lett.*, 2015, **15**, 4045.
164 L. Peng, D. Li, Z. Zhang, K. Huang, Y. Zhang, Z. Shi, R. Xie and W. Yang, *Nano Res.*, 2015, **8**, 3316.
165 D. Jo and H. Yang, *Chem. Commun.*, 2016, **52**, 709.
166 J. Kim, K. Lee, H. Kang, B. Park, J. Hwang, H. Jang, Y. Do and H. Yang, *Nanoscale*, 2015, **7**, 5363.
167 W. Song and H. Yang, *Chem. Mater.*, 2012, **24**, 1961.
168 P. Chuang, C. Lin and R. Liu, *ACS Appl. Mater. Interfaces*, 2014, **6**, 15379.
169 S. Park, A. Hong, J. Kim, H. Yang, K. Lee and H. Jang, *ACS Appl. Mater. Interfaces*, 2015, **7**, 6764.
170 H. Yoon, J. Oh, M. Ko, H. Yoo and Y. Do, *ACS Appl. Mater. Interfaces*, 2015, **7**, 7342.
171 C. Yoon, T. Kim, M. Shin, Y. Song, K. Shin, Y. Kim and K. Lee, *J. Mater. Chem. C*, 2015, **3**, 6908.
172 J. Kim, B. Kim, E. Jang, C. Han, J. Jo, Y. Do and H. Yang, *J. Mater. Chem. C*, 2017, **5**, 6755.
173 R. Boonsin, A. Barros, F. Donat, D. Boyer, G. Chadeyron, R. Schneider, P. Boutinaud and R. Mahiou, *ACS Photonics*, 2018, **5**, 462.
174 T. Jiang, M. Shen, P. Dai, M. Wu, X. Yu, G. Li, X. Xu and H. Zeng, *Nanotechnology*, 2017, **28**, 435702.
175 Z. Liu, Z. Guan, X. Li, A. Tang and F. Teng, *Adv. Opt. Mater.*, 2020, **8**, 1901555.
176 S. Palchoudhury, K. Ramasamy, R. Gupta and A. Gupta, *Front. Mater.*, 2019, **5**, 83.
177 P. Kulkarni, S. Nataraj, R. Balakrishna, D. Nagaraju and M. Reddy, *J. Mater. Chem. A*, 2017, **5**, 22040.
178 S. Madhusudanan, M. Kumar, K. Yasoda, D. Santhanagopalan and S. Batabyal, *J. Mater. Sci.: Mater. Electron.*, 2020, **31**, 752.
179 K. Ramasamy, R. K. Gupta, H. Sims, S. Palchoudhury, S. Ivanov and A. Gupta, *J. Mater. Chem. A*, 2015, **3**, 13263.
180 V. Mariappan, K. Krishnamoorthy, P. Pazhamalai, S. Sahoo, S. Nardekar and S. Kim, *Nano Energy*, 2019, **57**, 307.
181 P. Moraitis, R. Schropp and W. van Sark, *Opt. Mater.*, 2018, **84**, 636.
182 L. Bradshaw, K. Knowles, S. McDowall and D. Gamelin, *Nano Lett.*, 2015, **15**, 1315.
183 F. Meinardi, H. McDaniel, F. Carulli, A. Colombo, K. Velizhanin, N. Makarov, R. Simonutti, V. Klimov and S. Brovelli, *Nat. Nanotechnol.*, 2015, **10**, 878.
184 R. Sumner, S. Eiselt, T. Kilburn, C. Erickson, B. Carlson, D. Gamelin, S. McDowall and D. Patrick, *J. Phys. Chem. C*, 2017, **121**, 3252.
185 X. Liu, B. Luo, J. Liu, D. Jing, D. Benetti and F. Rosei, *J. Mater. Chem. A*, 2020, **8**, 1787.
186 M. Bergren, N. Makarov, K. Ramasamy, A. Jackson, R. Gughelmetti and H. McDaniel, *ACS Energy Lett.*, 2018, **3**, 520.
187 N. Makarov, K. Ramasamy, A. Jackson, A. Velarde, C. Castaneda, N. Archuleta, D. Hebert, M. Bergren and H. McDaniel, *ACS Nano*, 2019, **13**, 9112.
188 M. Choi, J. Yang, T. Hyeon and D. Kim, *npj Flexible Electron.*, 2018, **2**, 10.

